Experimental Quantum Networking Protocols via Four-Qubit Hyperentangled Dicke States

A. Chiuri,[1] C. Greganti,[1] M. Paternostro,[2] G. Vallone,[3] and P. Mataloni[1,4]

[1]*Dipartimento di Fisica, Sapienza Università di Roma, Piazzale Aldo Moro 5, I-00185 Roma, Italy*
[2]*Centre for Theoretical Atomic, Molecular, and Optical Physics, School of Mathematics and Physics,
Queen's University, Belfast BT7 1NN, United Kingdom*
[3]*Department of Information Engineering, University of Padova, I-35131 Padova, Italy*
[4]*Istituto Nazionale di Ottica (INO-CNR), Largo Enrico Fermi 6, I-50125 Firenze, Italy*

We report the experimental demonstration of two quantum networking protocols, namely quantum $1 \rightarrow 3$ telecloning and open-destination teleportation, implemented using a four-qubit register whose state is encoded in a high-quality two-photon hyperentangled Dicke state. The state resource is characterized using criteria based on multipartite entanglement witnesses. We explore the characteristic entanglement-sharing structure of a Dicke state by implementing high-fidelity projections of the four-qubit resource onto lower-dimensional states. Our work demonstrates for the first time the usefulness of Dicke states for quantum information processing.

Networking offers the benefits of connectivity and sharing, often allowing for tasks that individuals are unable to accomplish on their own. This is known for computing, where grids of processors outperform the computational power of single machines or allow the storage of much larger databases. It should thus be expected that similar advantages are transferred to the realm of quantum information. Quantum networking, where a given task is pursued by a lattice of local nodes sharing (possibly entangled) quantum channels, is emerging as a realistic scenario for the implementation of quantum protocols requiring medium or large registers. Key examples of such an approach are given by quantum repeaters [1], nonlocal gates [2], a scheme for light-mediated interactions of distant matter qubits [3], and one-way quantum computation [4].

In this scenario, photonics is playing an important role: the high reconfigurability of photonic setups and outstanding technical improvements have facilitated the birth of a new generation of experiments (performed both in bulk optics and, recently, in integrated photonic circuits [5]) that have demonstrated multiphoton quantum control towards high-fidelity computing with registers of a size inaccessible until only recently [6–11]. The design of complex interferometers and the exploitation of multiple degrees of freedom of a single photonic information carrier have enabled the production of interesting states, such as cluster or graph states, GHZ-like states and (phased) Dicke states [12–14], among others [15,16]. Dicke states have been successfully used to characterize multipartite entanglement close to fully symmetric states and its robustness to decoherence [14]. They are a potentially useful resource for the implementation of protocols for distributed quantum communication such as quantum secret sharing [17], quantum telecloning (QTC) [18], and open destination teleportation (ODT) [19,20]. So far, such opportunities

have only been examined theoretically and confirmed indirectly [12,13], leaving a full implementation of such protocols unaddressed.

In this Letter, we report the experimental demonstration of $1 \rightarrow 3$ QTC and ODT of logical states using a four-qubit symmetric Dicke state with two excitations realized using a high-quality hyperentangled (HE) photonic resource [14,21]. The entanglement-sharing structure of the state has been characterized quantitatively using a structural entanglement witness for symmetric Dicke states [22,23] and fidelity-based entanglement witnesses for the three- and two-qubit states achieved upon subjecting the Dicke register to proper single-qubit projections [13]. All such criteria have confirmed the theoretical expectations with a high degree of significance. As for the protocols themselves, the qubit state to teleclone or teleport is encoded in an extra degree of freedom of one of the physical information carriers entering such multipartite resource. This has been made possible by the use of a displaced Sagnac loop [24] [cf. Fig. 1], which introduced unprecedented flexibility in the setting, allowing for the realization of high-quality entangling two-qubit gates on heterogeneous degrees of freedom of a photon *within* the Sagnac loop itself. The high fidelities achieved between the experiments and theory (as large as 96%, on average, for ODT) demonstrate the usefulness of Dicke states as resources for distributed quantum communication beyond the limitations of a *proof of principle*. Our scheme is well suited for implementing $1 \rightarrow N > 3$ QTC of logical states or ODT with more than three receivers via the realization of larger HE resources, which is a realistic possibility.

Resource production and state characterization.—The building block of our experiment is the source of two-photon four-qubit polarization-path HE states developed in Refs. [21,25] and used recently to test multipartite
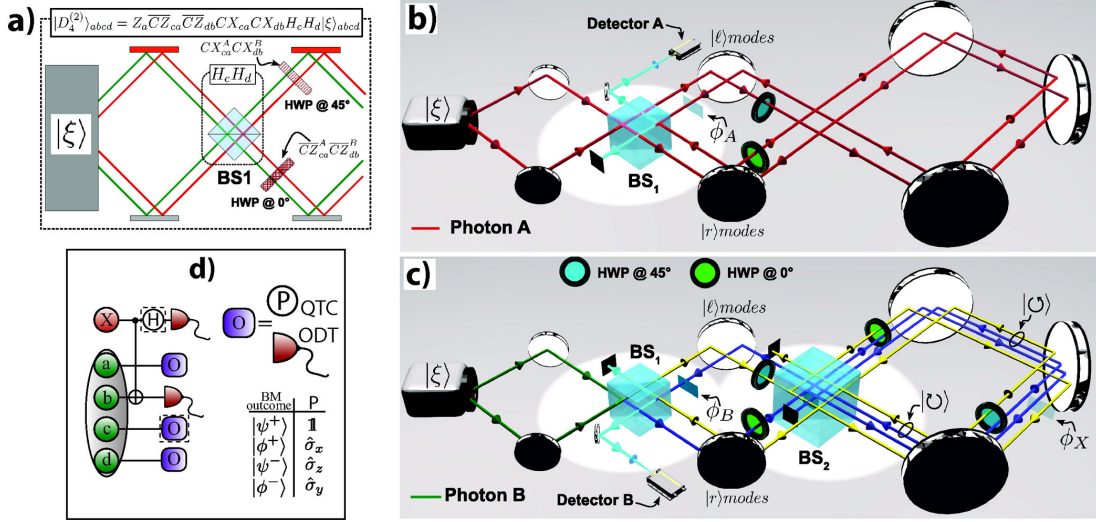
FIG. 1 (color online). (a) Scheme for the $|\xi\rangle \rightarrow |D_4^{(2)}\rangle$ conversion. The spatial qubits experience the Hadamard gates $\mathsf{H}_{c,d}$ implemented through a polarization insensitive beam splitter (BS_1). A controlled-NOT (controlled-PHASE) gate $\text{CX} = |0\rangle_i\langle 0| \otimes \mathbb{1}_j + |1\rangle_i\langle 1| \otimes \hat{\sigma}_j^x$ ($\overline{\text{CZ}} = |1\rangle_i\langle 1| \otimes \mathbb{1}_j + |0\rangle_i\langle 0| \otimes \hat{\sigma}_j^z$) is realized by a half-wave plate (HWP) with axis at $45°$ ($0°$) with respect to the vertical direction ($i = c, d, j = a, b$). The control (target) qubit of such gate is the path (polarization) degree of freedom (DOF). (b) and (c) Displaced Sagnac loop for the realization of the QTC/ODT protocol. Panel (b) [(c)] shows the path followed by the upper [lower] photon A [B]. The glass plates $\phi_{A,B,X}$ allow us to vary the relative phase between the different paths within the interferometer. (d) Circuit for $1 \rightarrow 3$ QTC and ODT. Qubits $\{a, b, c, d\}$ are prepared in $|D_4^{(2)}\rangle$ while X should be cloned or teleported. For QTC, the CX_{Xb} gate is complemented by the projection of X (b) on the eigenstates of σ^x (σ^z), so as to perform a BM. For QTC (ODT), operation O is a local Pauli gate P determined by the outcome of the BM according to the given table. For ODT (with, say, receiver qubit c), the operations in the dashed boxes should be removed.

entanglement, decoherence, and general quantum correlations [14,26,27]. Such an apparatus has been modified as described in the Supplemental Material [28] to produce the HE state $|\xi\rangle_{abcd} = [|HH\rangle_{ab}(|r\ell\rangle - |\ell r\rangle)_{cd} + 2|VV\rangle_{ab}|r\ell\rangle]_{cd}/\sqrt{6}$. Here, we have used the encoding $\{|H\rangle, |V\rangle\} \equiv \{|0\rangle, |1\rangle\}$, with H/V the horizontal/vertical polarization states of a single photon, and $\{|r\rangle, |\ell\rangle\} \equiv \{|0\rangle, |1\rangle\}$, where r and ℓ are the path followed by the photons emerging from the HE stage [28]. Qubits a, c (b, d) are encoded in the polarization and momentum of photon A (B). State $|\xi\rangle$ is turned into a four-qubit two-excitation Dicke state $|D_4^{(2)}\rangle = (1/\sqrt{6})\sum_{j=1}^6 |\Pi_j\rangle$ (with $|\Pi_j\rangle$ the elements of the vector of states constructed by taking all the permutation of 0's and 1's in $|0011\rangle$) by means of unitaries arranged as specified in Ref. [14] [cf. Fig. 1(a)]. In the basis of the physical information carriers, the state reads $|D_4^{(2)}\rangle = [|HH\ell\ell\rangle + |VVrr\rangle + (|VH\rangle + |HV\rangle) \times (|r\ell\rangle + |\ell r\rangle)]/\sqrt{6}$. The fidelity of the protocols depends on the quality of this state, as will be clarified soon. We have thus tested the closeness of the experimental state to $|D_4^{(2)}\rangle$ and characterized its entanglement-sharing structure.

First, we have ascertained the genuine multipartite entangled nature of the state at hand by using tools designed to assess the properties of symmetric Dicke states [22,23,29]. We have considered the multipartite entanglement witness

$$\mathcal{W}_m = [24\mathbb{1} + \hat{J}_x^2\hat{S}_x + \hat{J}_y^2\hat{S}_y + \hat{J}_z^2(31\mathbb{1} - 7\hat{J}_z^2)]/12, \quad (1)$$

which is specific of $|D_4^{(2)}\rangle$ [23] and requires only three measurement settings. Here, $\hat{S}_{x,y,z} = (\hat{J}_{x,y,z}^2 - \mathbb{1})/2$ with $\hat{J}_{x,y,z} = \sum_{i \in Q} \hat{\sigma}_i^{x,y,z}/2$ collective spin operators, $\hat{\sigma}^j$ ($j = x, y, z$) the j-Pauli matrix and $\mathcal{Q} = \{a, b, c, d\}$. The expectation value of $\mathcal{W}_m$ is positive on any biseparable four-qubit state; thus, negativity implies multipartite entanglement. Its experimental implementation allows us to provide a lower bound to the state fidelity with the ideal Dicke state as $F_{D_4^{(2)}} \geq (2 - \langle\mathcal{W}_m\rangle)/3$. When calculated over the resource that we have created in the lab, we achieve $\mathcal{W}_m = -0.341 \pm 0.015$, which leads to $F_{D_4^{(2)}} \geq (78 \pm 0.5)\%$. The genuine multipartite entangled nature of our state is corroborated by another significant test: we consider the witness testing biseparability on multipartite symmetric, permutation invariant states like our $|D_4^{(2)}\rangle$ [13,29]

$$\mathcal{W}_{\text{cs}}(\gamma) = b_4(\gamma)\mathbb{1} - (\hat{J}_x^2 + \hat{J}_y^2 + \gamma\hat{J}_z^2)(\gamma \in \mathbb{R}). \quad (2)$$

Here, $b_4(\gamma)$ is the maximum expectation value of the collective spin operator $\hat{J}_x^2 + \hat{J}_y^2 + \gamma\hat{J}_z^2$ over the class of biseparable states of four qubits and can be calculated for any value of the parameter γ [29]. Finding $\langle\mathcal{W}_{\text{cs}}(\gamma)\rangle < 0$ for some γ implies genuine multipartite entanglement. The direct evaluation shows that already for $\gamma = -0.12$ the witness is negative by more than one standard deviation and by more than fifteen for $\gamma = -2.5$ (cf. Supplemental Material [28]).

These results, although indicative of the high quality of the resource produced, are not exhaustive and further

evidence is needed. In order to provide an informed and experimentally not-demanding analysis on the state being generated, we have decided to resort to indirect yet highly significant evidence on its properties. In particular, we have exploited the interesting entanglement structure that arises from $|D_4^{(2)}\rangle$ upon subjecting part of the qubit register to specific single-qubit projections. In fact, by projecting one of the qubits onto the logical $|0\rangle$ and $|1\rangle$ states, we maintain or lower the number of excitations in the resulting state without leaving the Dicke space, respectively. Indeed, we achieve $|D_3^{(2)}\rangle = (|011\rangle + |101\rangle + |110\rangle)/\sqrt{3}$ when projecting onto $|0\rangle$, while $|D_3^1\rangle = (|100\rangle + |010\rangle + |001\rangle)/\sqrt{3}$ is obtained when the projected qubit is found in $|1\rangle$. Needless to say, these are genuinely tripartite entangled states, as it can be ascertained by using the entanglement witness formalism. For this task we have used the fidelity-based witness [30] $\mathcal{W}_{D_3^{(k)}} = (2/3)\mathbb{1} - |D_3^{(k)}\rangle\langle D_3^{(k)}|$ ($k = 1, 2$), whose mean is positive for any separable and biseparable three-qubit state, is $-1/3$ when evaluated over $|D_3^k\rangle$ and whose optimal decomposition (cf. Supplemental Material [28]) requires five local measurement settings [30,31]. We have implemented the witness for states obtained projecting qubit d (i.e., momentum of photon B), achieving $\langle \mathcal{W}_{D_3^{(1)}}^{\exp} \rangle = -0.21 \pm 0.01$ and $\langle \mathcal{W}_{D_3^{(2)}}^{\exp} \rangle = -0.24 \pm 0.01$ (the apex indicates their experimental nature) corresponding to lower bounds for the fidelity with the desired state of 0.876 ± 0.003 and 0.908 ± 0.003, respectively.

Finally, by projecting two qubits onto elements of the computational basis, one can obtain elements of the Bell basis. Indeed, regardless of the projected pair of qubits, $\langle ij|D_4^{(2)}\rangle = |\psi^+\rangle$ with $\{|\psi^\pm\rangle = (|01\rangle \pm |10\rangle)/\sqrt{2}, |\phi^\pm\rangle = (|00\rangle \pm |11\rangle)/\sqrt{2}\}$ the Bell basis and $i \neq j = 0, 1$. We have verified the quality of the reduced experimental states achieved by projecting the Dicke state onto $|10\rangle_{cd}$ and $|01\rangle_{cd}$ using two-qubit quantum state tomography (QST) [32] on the remaining two qubits. By finding fidelities >91% regardless of the projections operated, we can claim to have a very good Dicke resource, which puts us in the position to experimentally implement the quantum protocols.

$1 \rightarrow 3$ *QTC and ODT.*—Telecloning [18] is a communication primitive that merges teleportation and cloning to deliver approximate copies of a quantum state to remote nodes of a network. Differently, ODT [19] enables the teleportation of a state to an arbitrary location of the network. Both require shared multipartite entanglement. A deterministic version of ODT makes use of GHZ entanglement [20], while the optimal resources for QTC are symmetric states having the form of superpositions of Dicke states with k excitations [15,16,18,33]. Continuous-variable QTC was demonstrated in Ref. [34]. Although a symmetric Dicke state is known to be useful for such protocols (ODT being reformulated probabilistically) [12], no experimental demonstration has yet been reported: in Ref. [12], only an estimate of the efficiency of generation of a two-qubit Bell state between sender and receiver was

given, based on data for $|D_4^{(2)}\rangle$. Differently, our setup allows us to perform both QTC and probabilistic ODT.

We start discussing the $1 \rightarrow 3$ QTC scheme based on $|D_4^{(2)}\rangle$, which is a variation of the protocol given in Ref. [18]. We consider the qubit state to clone $|\alpha\rangle_X = \alpha|0\rangle_X + \beta|1\rangle_X(|\alpha|^2 + |\beta|^2 = 1)$, held by a *client X*. The agents of a *server* composed of qubits $\{a, b, c, d\}$ and sharing the Dicke resource agree on the identification of a *port* qubit p. The state of pair (X, p) undergoes a Bell measurement (BM) performed by implementing a controlled-NOT gate CX_{Xp} followed by a projection of X (b) on the eigenstates of $\hat{\sigma}^x$ ($\hat{\sigma}^z$). They publicly announce the results of their measurement, which leaves us with $\otimes_{j \in \mathcal{S}_{tc}} \mathsf{P}_j(\alpha|D_3^{(1)}\rangle + \beta|D_3^{(2)}\rangle)_{\mathcal{S}_{tc}} \otimes |\psi_+\rangle_{Xp}$, where $\mathcal{S}_{tc} = \{a, b, c, d\}/p$ is the set of server's qubits minus p, $|D_3^{(k)}\rangle$ is a three-qubit Dicke state with $k = 1, 2$ excitations and the gates P_j (identical for all the qubits in $\mathcal{S}_{tc}$) are determined by the outcome of the BM, as illustrated in Fig. 1(d). The protocol is now completed and the client's qubit is cloned into the state of the elements of $\mathcal{S}_{tc}$. To see this, we trace out two of the elements of such set and evaluate the state fidelity between the density matrix ρ_r of the remaining qubit r and the client's state, which reads $\mathcal{F}(\theta) = [9 - \cos(2\theta)]/12$, where $\alpha = \cos(\theta/2)$. Clearly, the fidelity depends on the state to clone, achieving a maximum (minimum) of $5/6$ ($2/3$) at $\theta = \pi/2$ ($\theta = 0$, π). This exceeds the value $7/9$ achieved by a universal symmetric $1 \rightarrow 3$ cloner due to the state-dependent nature of our protocol.

We now introduce the ODT protocol. As for QTC, this is formulated as a game with a client and a server. The client holds qubit X, into which the state $|\alpha\rangle_X$ to teleport is encoded. The elements of the server share the $|D_4^{(2)}\rangle$ resource. The client decides which party r of the server should receive the qubit to teleport (r and p can be any of $\{a, b, c, d\}$, and r is chosen at the last step of the scheme). Unlike QTC, the client performs a CX_{Xp}. At this stage the information on the qubit to teleport is spread across the server, and the client declares who will receive it. Depending on his choice, the members in $\mathcal{S}_{\text{odt}} = \{a, b, c, d\}/\{r, p\}$ project their qubits onto $|01\rangle_{\mathcal{S}_{\text{odt}}}$, getting $[\alpha(|001\rangle + |010\rangle)_{Xpr} + \beta(|111\rangle + |100\rangle)_{Xpr}] \otimes |01\rangle_{\mathcal{S}_{\text{odt}}}$. The scheme is completed by a projection onto $|+1\rangle_{Xp}$ with $|+\rangle = (|0\rangle + |1\rangle)/\sqrt{2}$ [35].

Experimental implementations of $1 \rightarrow 3$ *QTC.*—The setup in Figs. 1(b) and 1(c), which represent a significant improvement over the scheme used in Ref. [14], allows for the implementation of both the protocols. The shown displaced Sagnac loop and the use of the lower photon B allow us to add the client's qubit to the computational register. This is encoded in the sense of circulation of the loop by such field: modes $|r\rangle$ and $|\ell\rangle$ of photon B impinge on different points of beam splitter BS_2, so that the photon entering the Sagnac loop can follow the clockwise path, thus being in the $|\circlearrowright\rangle \equiv |0\rangle$ state, or the counterclockwise one, being in $|\circlearrowleft\rangle \equiv |1\rangle$ (photon A does not pass through

BS$_2$). The probability $|\alpha|^2$ of being in the former (latter) state relates to the transmittivity (reflectivity) of BS$_2$. This probability is varied using intensity attenuators intercepting the output modes of BS$_2$. At this stage, the state of the register is $|D_4^{(2)}\rangle_{abcd} \otimes (\alpha|\circlearrowleft\rangle + e^{i\phi_x}\sqrt{1-|\alpha|^2}|\circlearrowright\rangle)_X$, where ϕ_x is changed by tilting the glass plate in the loop. The CX$_{Xp}$ gate has been implemented with qubit X as the control, qubit b (i.e., the polarization of photon B) as the port p and taking a HWP rotated at 45° with respect to the optical axes, placed only on the counterclockwise circulating modes of the Sagnac loop [36]. The second passage of the lower photon in BS$_2$ allows us to project qubit X on the eigenstates of $\hat{\sigma}_X^x$. To complete the Bell measurement on qubits (X, p) we have placed a HWP and a PBS before the detector in order to project qubit p on the eigenstates of $\hat{\sigma}_p^z$. The remaining qubits $(a, c,$ and $d)$ embody three copies of the qubit X. Their quality has been tested by performing QST over the reduced states obtained by tracing over any two qubits. Pauli operators in the path DOF have been measured using the second passage of both photons through BS$_1$. The glass plates $\phi_{A,B}$ allowed projections onto $\frac{1}{\sqrt{2}}(|r\rangle + e^{i\phi_{A(B)}}|\ell\rangle)_{c(d)}$. To perform QST on the polarization DOF we used an analyzer composed of HWP, QWP and PBS before the photodetector. To trace over polarization, we removed the analyzer. To trace over the path, a delayer was placed on either $|r\rangle$ or $|\ell\rangle$ coming back to BS$_1$, thus making them distinguishable and spoiling their interference.

While in the Supplemental Material [28] we show the performance of our QTC machine for the specific case of the input state $|1\rangle_X$ (with $p = b$), it is worth stressing that our setup allows us to teleclone arbitrary input states. To illustrate the working principles and efficiency of the telecloning machine, we have considered the logical states $|0\rangle_X$ and $|+\rangle_X$ and $|1\rangle_X$ (i.e., we took $\theta \simeq 0, \pi/2$ and π) and measured the corresponding copies in qubit a (i.e., the polarization of photon A). States $|0\rangle_X$ and $|1\rangle_X$ were generated by selecting the modes in the displaced Sagnac. In the first (second) case we considered only modes $|\circlearrowleft\rangle$ $(|\circlearrowright\rangle)$, while $|+\rangle_X$ was generated using both modes and adjusting the relative phase with the glass-plate ϕ_X (by varying this phase, we can explore the whole phase-covariant case). Although the experimental results are very close to the expectations for $\mathcal{F}(\theta)$ [cf. Fig. 2(b)], some discrepancies are found for $\theta = \pi/2$. In particular, the theory seems to underestimate (overestimate) the experimental fidelity of telecloning close to $\theta = \pi/2$ $(\theta = 0, \pi)$. These effects are due to the mixedness of the X state entering the Sagnac loop as well as the suboptimal fidelity between the experimental resource and $|D_4^{(2)}\rangle$. In fact, the experimental input state corresponding to $\theta \simeq \pi/2$ has fidelity 0.91 ± 0.02 with the desired $|+\rangle_X$ due to depleted off-diagonal elements in its density matrix (cf. Supplemental Material [28]). We have thus modeled the telecloning of dephased client states based on the use of a mixed Dicke channel of subunit fidelity with $|D_4^{(2)}\rangle$. The details are

presented in Ref. [28]. Here we mention that, by including the uncertainty associated with the estimated $F_{D_4^{(2)}}$, we have determined a θ-dependent region of telecloning fidelities into which the fidelity between the experimental state of the clones and the input client state falls. As shown in Fig. 2(b), this provides a better agreement between theory and data.

Experimental implementations of ODT.—In ODT the client holds qubit X, which is added to the computational register using the Sagnac loop. The client's qubit has been teleported to the server's elements a and b (i.e., the polarization of photons A and B). The necessary CX$_{Xp}$ gate has been implemented, as above, by taking X as the control and $p = b$ as the target qubit. The server's elements $\{c, d\}$ have been projected onto $|01\rangle_{cd}$ and $|10\rangle_{cd}$. Depending on the chosen receiver (either a or b), the scheme is implemented by projecting onto $|+1\rangle_{Xa(b)}$ and performing QST of the teleported qubit $b(a)$. While the projection onto $|+\rangle_X$ has been realized using the second passage of the lower photon through BS$_2$, a projection onto $|1\rangle_{a(b)}$ is achieved projecting the physical qubit onto $|V\rangle_{a(b)}$. In Table I we report the experimental results obtained for several measurement configurations and teleportation channels. In Supplemental Material [28] we provide the reconstructed density matrices of qubits $\{X, a, b\}$ for each configuration used.

Conclusions and outlook.—We have implemented QTC and ODT of logical states using a four-qubit symmetric Dicke state. We have realized a novel setup based on the well-tested HE polarization-path states and complemented by a displaced Sagnac loop. This allowed the encoding of nontrivial input states in the computational register, and the performance of high-quality quantum gates and protocols. Our results go beyond state-of-the-art in the manipulation
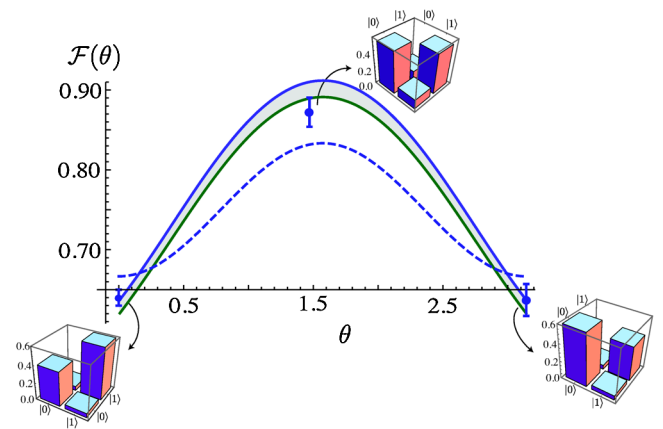

FIG. 2 (color online).   Theoretical QTC fidelity and experimental density matrices of the clone (qubit a) for various input states. We show the fidelities between the experimental input states and clones (associated uncertainties determined by considering Poissonian fluctuations of the coincidence counts). The dashed line shows the theoretical fidelity for pure input states of the client's qubit. The dashed area encloses the values of the fidelity achieved for a mixed input state of X and the use of an imperfect Dicke resource compatible with the states generated in our experiment (cf. Supplemental Material [28]).

TABLE I. Experimental fidelities between the teleported qubit (a or b) and the state of qubit X (determined by θ). Uncertainties result from associating Poissonian fluctuations to the coincidence counts.

Projection	θ	Fidelity	Projection	θ	Fidelity
$_{cd}\langle 10|$	0	$\mathcal{F}_a = 0.93 \pm 0.01$	$_{cd}\langle 01|$	π	$\mathcal{F}_a = 0.98 \pm 0.01$
$_{cd}\langle 10|$	0	$\mathcal{F}_b = 0.95 \pm 0.01$	$_{cd}\langle 01|$	π	$\mathcal{F}_b = 0.97 \pm 0.01$
$_{cd}\langle 01|$	0	$\mathcal{F}_a = 0.97 \pm 0.01$	$_{cd}\langle 10|$	1.46	$\mathcal{F}_a = 0.92 \pm 0.02$
$_{cd}\langle 01|$	0	$\mathcal{F}_b = 0.97 \pm 0.01$	$_{cd}\langle 10|$	1.46	$\mathcal{F}_b = 0.98 \pm 0.01$
$_{cd}\langle 10|$	π	$\mathcal{F}_a = 0.96 \pm 0.01$	$_{cd}\langle 01|$	1.37	$\mathcal{F}_a = 0.97 \pm 0.02$
$_{cd}\langle 10|$	π	$\mathcal{F}_b = 0.98 \pm 0.01$	$_{cd}\langle 01|$	1.37	$\mathcal{F}_b = 0.96 \pm 0.02$

of experimental Dicke states and the realization of quantum networking.

[1] A. I. Lvovsky, B. C. Sanders, and W. Tittel, Nature Photon. **3**, 706 (2009), and references therein.

[2] D. Gottesman and I. Chuang, Nature (London) **402**, 390 (1999); J. Eisert, K. Jacobs, P. Papadopoulos, and M. B. Plenio, Phys. Rev. A **62**, 052317 (2000); D. Collins, N. Linden, and S. Popescu, *ibid.* **64**, 032302 (2001); S. F. Huelga, M. B. Plenio, and J. A. Vaccaro, *ibid.* **65**, 042316 (2002); M. Paternostro, M. S. Kim, and G. M. Palma, J. Mod. Opt. **50**, 2075 (2003).

[3] H. J. Kimble, Nature (London) **453**, 1023 (2008); B. B. Blinov, D. L. Moehring, L.-M. Duan, and C. Monroe, *ibid.* **428**, 153 (2004); S. Olmschenk, D. N. Matsukevich, P. Maunz, D. Hayes, L.-M. Duan, and C. Monroe, Science **323**, 486 (2009).

[4] H. J. Briegel, D. E. Browne, W. Dür, R. Raussendorf, and M. Van den Nest, Nat. Phys. **5**, 19 (2009).

[5] A. Politi, M. J. Cryan, J. G. Rarity, S. Yu, and J. L. O'Brien, Science **320**, 646 (2008); A. Politi, J. C. F. Matthews, and J. L. O'Brien, *ibid.* **325**, 1221 (2009); L. Sansoni, F. Sciarrino, G. Vallone, P. Mataloni, A. Crespi, R. Ramponi, and R. Osellame, Phys. Rev. Lett. **105**, 200503 (2010); A. Crespi, R. Ramponi, R. Osellame, L. Sansoni, I. Bongioanni, F. Sciarrino, G. Vallone, and P. Mataloni, Nature Commun. **2**, 566 (2011).

[6] W.-B. Gao, P. Xu, X.-C. Yao, O. Gühne, A. Cabello, C.-Y. Lu, C.-Z. Peng, Z.-B. Chen, and J.-W. Pan, Phys. Rev. Lett. **104**, 020501 (2010).

[7] G. Vallone, E. Pomarico, F. DeMartini, and P. Mataloni, Phys. Rev. Lett. **100**, 160502 (2008).

[8] C.-Y. Lu, X.-Q. Zhou, O. Gühne, W.-B. Gao, J. Zhang, Z.-S. Yuan, A. Goebel, T. Yang, and J.-W. Pan, Nat. Phys. **3**, 91 (2007).

[9] G. Vallone, G. Donati, N. Bruno, A. Chiuri, and P. Mataloni, Phys. Rev. A **81**, 050302(R) (2010).

[10] D. N. Biggerstaff, R. Kaltenbaek, D. R. Hamel, G. Weihs, T. Rudolph, and K. J. Resch, Phys. Rev. Lett. **103**, 240504 (2009).

[11] W. B. Gao, C.-Y. Lu, X.-C. Yao, P. Xu, O. Gühne, A. Goebel, Y.-A. Chen, C.-Z. Peng, Z.-B. Chen, and J.-W. Pan, Nat. Phys. **6**, 331 (2010).

[12] N. Kiesel, C. Schmid, G. Toth, E. Solano, and H. Weinfurter, Phys. Rev. Lett. **98**, 063604 (2007).

[13] R. Prevedel, G. Cronenberg, M. Tame, M. Paternostro, P. Walther, M. Kim, and A. Zeilinger, Phys. Rev. Lett. **103**, 020503 (2009); W. Wieczorek, R. Krischek, N. Kiesel, P. Michelberger, G. Tóth, and H. Weinfurter, Phys. Rev. Lett. **103**, 020504 (2009).

[14] A. Chiuri, G. Vallone, N. Bruno, C. Macchiavello, D. Bruß, and P. Mataloni, Phys. Rev. Lett. **105**, 250501 (2010).

[15] M. Radmark, M. Żukowski, and M. Bourennane, Phys. Rev. Lett. **103**, 150501 (2009); New J. Phys. **11**, 103016 (2009).

[16] M. Bourennane, M. Eibl, S. Gaertner, N. Kiesel, C. Kurtsiefer, and H. Weinfurter, Phys. Rev. Lett. **96**, 100502 (2006).

[17] M. Hillery, V. Bužek, and A. Berthiaume, Phys. Rev. A **59**, 1829 (1999).

[18] M. Murao, D. Jonathan, M. B. Plenio, and V. Vedral, Phys. Rev. A **59**, 156 (1999).

[19] A. Karlsson and M. Bourennane, Phys. Rev. A **58**, 4394 (1998).

[20] Z. Zhao, Y.-A. Chen, A.-N. Zhang, T. Yang, H. J. Briegel, and J.-W. Pan, Nature (London) **430**, 54 (2004).

[21] M. Barbieri, C. Cinelli, P. Mataloni, and F. DeMartini, Phys. Rev. A **72**, 052110 (2005).

[22] P. Krammer, H. Kampermann, D. Bruß, R. Bertlmann, L. Kwek, and C. Macchiavello, Phys. Rev. Lett. **103**, 100502 (2009).

[23] G. Töth, W. Wieczorek, R. Krischek, N. Kiesel, P. Michelberger, and H. Weinfurter, New J. Phys. **11**, 083002 (2009).

[24] M. P. Almeida, F. de Melo, M. Hor-Meyll, A. Salles, S. P. Walborn, P. H. S. Ribeiro, and L. Davidovich, Science **316**, 579 (2007).

[25] R. Ceccarelli, G. Vallone, F. DeMartini, P. Mataloni, and A. Cabello, Phys. Rev. Lett. **103**, 160401 (2009).

[26] A. Chiuri, G. Vallone, M. Paternostro, and P. Mataloni, Phys. Rev. A **84**, 020304(R) (2011).

[27] A. Chiuri, L. Mazzola, M. Paternostro, and P. Mataloni, New J. Phys. **14**, 085006 (2012).

[28] See Supplemental Material at http://link.aps.org/supplemental/10.1103/PhysRevLett.109.173604 for an additional analysis on the properties of the system.

[29] S. Campbell, M. S. Tame, and M. Paternostro, New J. Phys. **11**, 073039 (2009).

[30] A. Acín, D. Bruss, M. Lewenstein, and A. Sanpera, Phys. Rev. Lett. **87**, 040401 (2001).

[31] O. Gühne and P. Hyllus, Int. J. Theor. Phys. **42**, 1001 (2003).

[32] D. F. V. James, P. G. Kwiat, W. J. Munro, and A. G. White, Phys. Rev. A **64**, 052312 (2001).

[33] F. Ciccarello, M. Paternostro, S. Bose, D. Browne, G. Palma, and M. Zarcone, Phys. Rev. A **82**, 030302(R) (2010).

[34] S. Koike, H. Takahashi, H. Yonezawa, N. Takei, S. Braunstein, T. Aoki, and A. Furusawa, Phys. Rev. Lett. **96**, 060504 (2006).

[35] Similar results hold for projections onto $|10\rangle_{\mathcal{S}_{\text{odt}}}$.

[36] The second HWP in Fig. 1(d) compensates the temporal delay introduced by the first one.